Design and Characterization of an Open-source Robotic Leg Prosthesis

Alejandro F. Azocar, *Student Member, IEEE*, Luke M. Mooney, Levi J. Hargrove, *Member, IEEE*, and Elliott J. Rouse, *Member, IEEE*

***Abstract*—Challenges associated with current prosthetic technologies limit the quality of life of lower-limb amputees. Passive prostheses lead amputees to walk slower, use more energy, fall more often, and modify their gait patterns to compensate for the prosthesis' lack of net-positive mechanical energy. Robotic prostheses can provide mechanical energy, but may also introduce challenges through controller design. Fortunately, talented researchers are studying how to best control robotic leg prostheses, but the time and resources required to develop prosthetic hardware has limited their potential impact. Even after research is completed, comparison of results is confounded by the use of different, researcher-specific hardware. To address these issues, we have developed the Open-source Leg (OSL): a scalable robotic knee/ankle prosthesis intended to foster investigations of control strategies. This paper introduces the design goals, transmission selection, hardware implementation, and initial control benchmarks for the OSL. The OSL provides a common hardware platform for comparison of control strategies, lowers the barrier to entry for prosthesis research, and enables testing within the lab, community, and at home.**

I. Introduction

Over one million lower-limb amputees live in the United States, and their quality of life is affected by the performance of today's prostheses [1]. Most amputees walk slower, use more energy, and are less stable than able-bodied individuals [2]–[4]. In part, these deficits stem from the passive nature of traditional prosthetic legs; that is, most leg prostheses cannot provide net-positive mechanical energy, which contrasts with the abilities of the human neuromuscular system [5]. Without added mechanical energy, certain activities are especially challenging for individuals with amputations, including stair and ramp ascent [6]. Furthermore, to compensate for the lack of mechanical energy, amputees often adopt an asymmetrical gait pattern and significantly modify the biomechanics and muscle activity of other joints, such as the hip [7], [8]. Compensatory changes to gait mechanics can lead to further complications, including osteoarthritis, osteoporosis, and back pain [9]. Thus, restoring appropriate gait characteristics requires robotic leg prostheses that are safe, stable, and intuitively controlled.

Over the past decade, many encouraging robotic leg prostheses have been developed [10]–[13]. Three generations of knee-ankle prostheses were created at Vanderbilt University. The original design was pneumatically powered, and, after several revisions, the current prosthesis uses electric motors and a belt/chain transmission [14], [15]. In addition, investigators at the Massachusetts Institute of Technology (MIT) developed robotic ankle and knee systems independently. The robotic ankle utilized series and parallel elasticity and was commercialized by BiOM, and now Ottobock [16]. Their robotic knee prosthesis used a clutchable series-elastic actuator (CSEA) for minimal electrical energy consumption [17]. Finally, researchers at Arizona State University developed a spring ankle with regenerative kinetics (SPARKy), which integrated an electric motor, lead screw, and a series spring [18]. Many other research groups, some who focus on prosthesis control, have also developed promising robotic prostheses and emulators [19]–[23].

While the design of high-performance robotic leg prostheses is challenging, development of intelligent control systems is especially difficult. Prosthesis control systems must accomplish multiple tasks, such as recognizing the amputee's intended movements (high-level control), applying an appropriate control law based on the amputee's intent (mid-level control), and using local feedback to command the actuation systems within the prosthesis (low-level control) [24]. Controller complexity increases further during simultaneous control of both knee and ankle joints [25]. Researchers have developed control systems capable of controlling multiple joints across various ambulation modes (level ground walking, ramp ascent/descent, stair ascent/descent); however, these control strategies are highly sophisticated, sometimes containing over 100 parameters and requiring hours of tuning [26]. Before robotic legs can realize their full potential for clinical impact, future work is needed in the control of these systems.

The lack of open, available prosthetic hardware has limited the impact of the field, particularly with respect to intuitive, seamless control systems. A number of researchers around the world are independently developing robotic prostheses on which to test their control strategies; however, this development requires a substantial level of time and financial resources. Thus, this high investment may preclude

*This work was supported by the National Science Foundation (NSF) Graduate Research Fellowship under Grant No. DGE-1324585, NSF National Robotics Initiative (NRI) under Grant No. CMMI 1734586, and the MSL Renewed Hope Foundation.

A. F. Azocar is with the Department of Mechanical Engineering, University of Michigan, and also with the Neurobionics Lab, University of Michigan (e-mail: afazocar@umich.edu).

Luke M. Mooney is with Dephy, Inc., Boston, MA 02129 USA (e-mail: lmooney@dephy.com).

Levi J. Hargrove is with the Departments of Physical Medicine and Rehabilitation, and Biomedical Engineering, Northwestern University, Evanston, IL 60208 USA, and also with the Center for Bionic Medicine, Shirley Ryan AbilityLab, Chicago, IL 60611 USA (e-mail: l-hargrove@northwestern.edu).

E. J. Rouse is with the Department of Mechanical Engineering and the Robotics Institute, University of Michigan, Ann Arbor, MI 48109 USA, and also with the Neurobionics Lab, University of Michigan, Ann Arbor, MI 48109 USA (phone: 734-763-3629; e-mail: ejrouse@umich.edu).

talented researchers in related fields, such as bipedal robotics, from applying their research to prostheses. Furthermore, even after research is completed, the differences in mechanical designs and performance can hinder comparisons. Researchers use different prostheses that vary widely in size, weight, transmission design, controllability, and degrees of freedom. Additionally, many research groups use prostheses that must be tethered to a power supply, limiting their research to within the laboratory. Low-cost, open-source prosthetic hardware and software will enable more researchers to enter the prosthetics field, improve comparison of control strategies, and promote worldwide collaboration to improve amputee quality of life.

In this paper, we introduce the Open-source Leg (OSL): a robotic leg prosthesis that facilitates control system development and comparison [27]. We present the overarching design objectives, transmission selection, hardware implementation, and characterization in the time and frequency domains. The intent of the OSL is to offer a common hardware platform for comparison of control strategies, lower the barrier to entry for prosthesis research, and enable testing within the lab, community, and at home.

II. Design

A. Design Objectives

The overall goal of the OSL (Fig. 1) is to provide a common hardware platform that streamlines the development and testing of robotic leg prostheses. The OSL includes the prosthesis hardware, sensors, low-level control software, and an Application Peripheral Interface (API) to communicate with researchers' preferred high-level control systems. We have developed several characteristics that have guided the overarching design:

1. *Simple*: the leg does not require high-precision machine components (*e.g.*, ball or roller screws) and can be easily assembled and disassembled. All hardware components are machined by a single manufacturer.

2. *Portable*: the prosthesis is lightweight and does not require a tether to a power supply. Each joint has its own onboard battery, allowing researchers to use the prosthesis outside of the laboratory easily.

3. *Scalable*: the ankle and knee operate independently, enabling researchers to work with both transtibial and transfemoral amputees, in single and dual joint configurations. Control strategies can be implemented in a single embedded system that operates both joints.

4. *Customizable*: the knee joint is selectable series-elastic, and can be configured with varying amounts of series elasticity (or none at all). In addition, the ankle can use both low-profile and flat feet, giving researchers flexibility while still providing a common platform.

5. *Economical*: the prosthesis is estimated to cost $10,000-$25,000, depending on degrees of freedom, series-elastic configuration, and sensing options.

Fig. 1. Rendering (top) and physical implementation (bottom) of the OSL.

B. Transmission Design

To investigate potential prosthesis designs, able-bodied locomotion data were obtained from the literature. Data from walking at slow, self-selected, and fast speeds, in addition to data from ascending/descending stairs, were used [28]. These data yielded insight into the prosthesis' kinetic, kinematic, and electromechanical requirements, across a range of transmission ratios and stiffness coefficients for the series elasticity. The associated torque/velocity, and accompanying current/voltage requirements were used as the foundation for the mechanical design decisions [17].

To simplify manufacturing, assembly, and control, the knee and ankle joints follow similar design strategies. Both joints use an electric motor coupled to a multi-stage belt drive transmission, increasing the torque provided at the output. Timing belt drives were chosen for their simplicity, low weight, low cost, and quiet operation. The transmission stages were designed to be as compact as possible while resisting tooth jump during peak torque. Newly developed PowerGrip GT3 (Stock Drive Products/Sterling Instrument, Hicksville, NY, USA) belts were chosen because they provide longer belt life, increased load-carrying capacity, and quieter operation relative to other available belts [29]. Design specifications that relate transmission geometry (*i.e.*, tooth

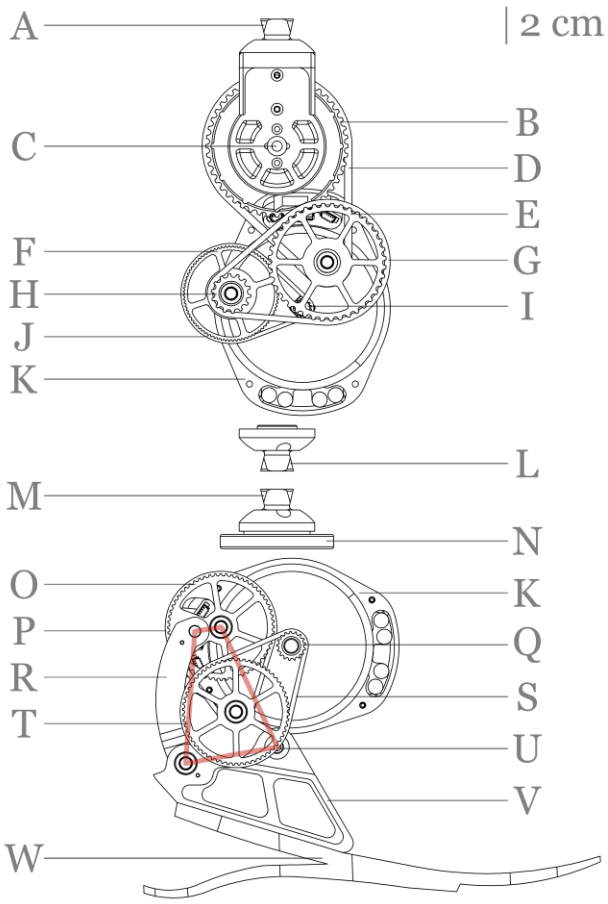

Fig. 2. Major components of the OSL: (A) proximal pyramid, knee; (B) 3rd stage output pulley, knee; (C) knee joint; (D) 3rd stage belt, knee; (E) 2nd stage output pulley (coupled to 3rd stage input pulley), knee; (F) 1st stage output pulley, knee; (G) 2nd stage belt, knee; (H) 2nd stage input pulley, knee; (I) 1st stage input pulley, knee; (J) 1st stage belt, knee; (K) Dephy actuator; (L) distal pyramid, knee; (M) proximal pyramid, ankle; (N) SRI load cell; (O) 2nd stage output pulley, ankle; (P) 2nd stage belt, (ankle); (Q) 1st stage input pulley, ankle; (R) linkage coupler; (S) 1st stage belt, ankle; (T) 1st stage output pulley (coupled to 2nd stage input pulley), ankle; (U) ankle joint; (V) linkage rocker and foot attachment; (W) Össur LP Vari-Flex foot. The ankle's virtual four-bar linkage is highlighted.

profile, number of teeth of each pulley, pulley center-to-center distance, and belt width) to rated tooth jump torque were not readily available; however, the manufacturer's documentation includes tooth jump resistance data that yielded some insight into tooth jump characteristics [29]. The force per unit belt width that endangers tooth jump for 2, 3, and 5 mm pitch GT3 belts was estimated to be approximately 29, 46, and 151 N/mm, respectively. These forces were used to specify minimum belt widths at each stage of the transmissions. Finally, the geometric configurations of the belt drive transmissions were determined by investigating the following parameters: overall transmission volume, number of belt stages, pitch of each belt stage, width of each stage, number of teeth engaged, ease of assembly, and availability of belt lengths and widths.

C. Knee Overview

Following analysis of the desired kinetic and kinematic requirements, a target transmission ratio of 49:1 was chosen (final transmission ratio of 49.4:1). This transmission ratio allows the knee to achieve the torques and velocities required for locomotion while maintaining acceptable voltage and current requirements. A heuristic design exploration (see Section II-B) resulted in a three-stage belt drive transmission consisting of a 2 mm pitch stage and two 5 mm pitch stages (Fig. 2). Transmission components are machined from 7075-T6 Aluminum through a combination of subtractive manufacturing and wire electronic discharge machining. Detailed knee specifications are available in Table I.

TABLE I
OSL DESIGN AND CONTROL SPECIFICATIONS

Metric	Knee	Ankle
Transmission Ratio[a]	49.4	58.4 ± 16.0
Series Elasticity (Nm/rad)	100-600	-
Range of Motion (º)	120	30
Mass[b,c] (g)	2160-2331	1739
Height (mm)	240	213
Width (mm)	110	94
Position Rise Time (ms)	25.6 ± 8.7	
Position Overshoot (%)	2.4 ± 3.9	
Position Steady-state Error (%)	0.9 ± 1.5	
Position Bandwidth (Hz)	~10-20	
Current Rise Time (ms)	29.2 ± 15.6	
Current Overshoot (%)	18.5 ± 11.3	
Current Steady-state Error (%)	0.1 ± 0.6	
Current Bandwidth (Hz)	> 200	
Peak Torque, Continuous[d] (Nm)	~47	
Peak Torque, Instantaneous[d] (Nm)	~140	
Bus Voltage (V)	36	
Peak Bus Current (A)	Fused at 30	
Torque Constant (Nm/A)	0.096	
Motor Constant (Nm/W$^{1/2}$)	0.23	

a. See Fig. 4 for ankle transmission ratio profile.
b. Includes motor and battery mass.
c. Knee mass varies with SEA configuration.
d. Assuming a transmission ratio of 49.4:1.

D. Selectable Series Elasticity

Many researchers require series-elastic actuators (SEA), and our knee design includes the ability to configure the mechanism as an SEA, with options for a range of stiffness coefficients (including a non-SEA configuration). This ability to configure the SEA is termed *selectable series elasticity.* In assistive technologies and other areas of robotics, series elasticity is often implemented for improved torque control, shock tolerance, and the ability to store and return energy [30]. However, some researchers prefer to forgo the SEA configuration due to the added weight and complexity.

In our knee design, series elasticity is achieved using custom torsional spring disks (Fig. 3, left). Each disk is 4.3 mm thick and designed with 24 parallel, radially cantilevered beams that can deflect up to 15º. When maximally deflected, the peak von Mises stress is approximately 250 MPa (about half of the yield strength). The torsional spring disks are intended to be used with an inner gear-shaped shaft. The shaft has teeth that interface with the tip of each cantilever. Relative motion between the inner gear and spring disk deflects the cantilevered beams primarily through rolling contact, resulting in efficient energy storage. Overall, this

Fig. 3. Front view of an individual spring disk (left), exploded view of the spring disks stacked inside the knee output pulley (middle), and torque-angle relationship of the knee at various levels of series elasticity (right).

torsion spring implementation enables a compact, lightweight, SEA with easily modifiable stiffness properties.

Up to six spring disks can be used in parallel, depending on the desired stiffness coefficient of the series elasticity. When characterized within the knee design, the spring disks had a mean stiffness of 97 ± 20 Nm/rad (Fig. 3, right); the hysteresis shown in the torque-angle profiles of the spring configurations is due to energy loss in the belt transmission stages (in series with the series elasticity). The spring disks are stacked inside the 3rd stage output pulley (Fig. 3, middle), enabling a compact design with no added volume for the series elastic element. With up to six parallel spring disks, series stiffness values from approximately 100 Nm/rad to 600 Nm/rad can be achieved. The non-SEA configuration is obtained by using a separate output pulley setup without springs.

E. Ankle Overview

The ankle design was based on the robotic knee hardware; however, a fundamental difference is that the ankle prosthesis uses a two-stage timing belt drive transmission coupled to a four-bar linkage mechanism (Fig. 2). A four-bar linkage was chosen to reduce the overall size/height of the ankle prosthesis. Motion of the linkage is driven by rotation of the 2nd stage output pulley and results in rotation of the ankle joint. The angle of the linkage rocker (Fig. 2, V) corresponds to the angle of the ankle joint. Additionally, the rocker couples the transmission to a prosthetic foot. Two rockers are available, one for a commercially available low-profile foot (model: VLPE5250, Össur Americas), and another for a custom flat foot (not shown).

The addition of a four-bar linkage to the ankle's transmission resulted in a kinematically-varying transmission ratio. Therefore, the locomotion-based kinetic and kinematic analysis was modified to determine a range of acceptable transmission ratios; the analysis determined that peak performance occurred at transmission ratios between 40:1 and 60:1. The design of the ankle transmission included the design parameters for the timing belts (see Section II-B), in addition to rocker (ankle joint) range of motion, transmission ratio variability, and relative link lengths. Simulations of the available belt, pulley, and linkage configurations were developed to aid in selecting the final design, which consists of two 3 mm pitch belt stages and a four-bar linkage with a 30º range of motion. The final transmission ratio remains within the target range (40-60:1) for most of the ankle's range of motion (Table I, Fig. 4) [11], [15], [31]. Due to size and complexity constraints, the ankle does not include series elasticity; however, the ankle can be coupled to a carbon fiber foot, which provides some of the benefits of series elasticity without the added size and complexity.

F. Structural Support

The transmissions of each prosthesis joint are contained within clamshell-style housings (Fig. 1). The clamshell-style design—two halves that are fastened together—simplifies the assembly process and reduces pinch points that may lead to user or researcher injury. The housings locate the timing pulleys as well as provide structural support for the prosthesis. In addition, the housings incorporate a simple belt tensioning system that enables minor modifications to the distances between pulley shafts. Appropriate belt tensioning is necessary to ensure maximum torque capacity of the belt drive transmission. Mechanical hard stops are integrated into the housings to ensure that the OSL cannot rotate to biomechanically unsafe positions. Finally, the housings include space for batteries and electronics, creating a self-contained, portable prosthesis.

G. Mechatronics and Control

To provide mechanical power, the OSL utilizes a brushless electric motor at each joint. Originally developed for the drone industry, high-torque, exterior rotor motors were selected based on their high specific power, and high

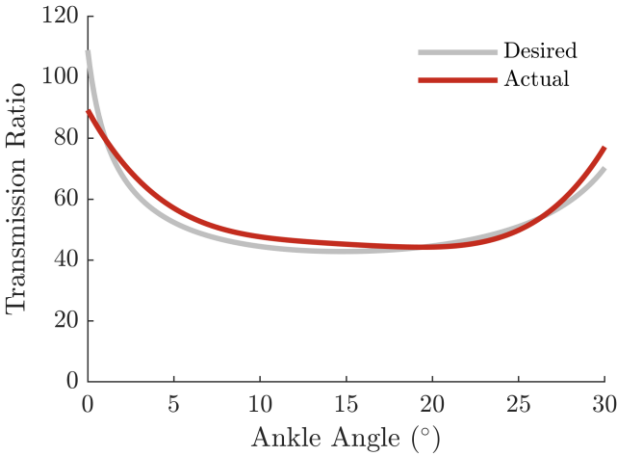

Fig. 4. Ankle transmission ratio throughout the range of motion.

motor constant (model: U8-16, T-motor, Nanchang, Jiangxi, China). The motors were custom modified by Dephy Inc. (Boston, MA, USA), who also developed the brushless drive electronics. Dephy actuation technology implements Field Oriented Control commutation for the 21 pole pairs in the motors and is based on an open-source embedded platform. The Dephy brushless drive's embedded architecture stems from the Flexible, Scalable Electronics Architecture (FlexSEA), an open-source brushless drive and motor controller developed for wearable robotic applications [32], [33]. Feedback loops are closed within the brushless drive at 1 kHz and 10 kHz for position and current, respectively. Onboard sensing within the drive includes electrical states of the motor windings and bus, as well as a nine-axis inertial measurement unit (model: MPU-9250, InvenSense, San Jose, CA, USA), temperature sensing, and a 14-bit absolute motor encoder (model: AS5047P, ams AG, Premstaetten, Austria). Depending on the application, peripheral electrical hardware can communicate with the brushless drive via Inter-Integrated Circuit (I^2C) and other forms of communication. The ankle and knee joints each have a 14-bit absolute encoder that is sampled at 1 kHz (model: AS5048B, ams AG, Premstaetten, Austria). In addition, a custom, embedded six-channel amplifier and 16-bit analog to digital converter are used to obtain data from an integrated six-axis load sensor at 1 kHz (model: M3554E, Sunrise Instruments, Nanning, China). The brushless drives receive reference commands and controller parameters (*e.g.*, desired position, desired current, controller gains, *etc.*) via Universal Serial Bus (USB) or Serial Peripheral Interface (SPI) communication, sent from a higher-level control system.

Overall prosthesis behavior is intended to be governed by a higher-level control system developed by researchers. In our application, control system commands are sent from a single-board computer (model: Raspberry Pi 3, Raspberry Pi Foundation, Cambridgeshire, UK), using a custom API developed for Python. However, other researchers are free to use different hardware implementations for the higher-level control system, utilizing the API. Communication between the higher-level control system and the brushless drive occurs at approximately 350-1000 Hz, depending on the communication protocol chosen by the researcher.

Electrical power is supplied onboard for each joint, enabling testing outside the laboratory. Thus, there are two identical batteries; two separate electrical power sources were chosen to permit the use of each joint independently. The power sources are 36 V lithium polymer (LiPo) batteries with a capacity of 950 mAH (model: 25087X2, Venom Power, Rathdrum, ID, USA).

III. Characterization Methods

The electromechanical performance of the OSL was characterized in the time and frequency domains. The time and frequency domain tests were completed for both position and current control systems. During testing of the current control system, the actuator was fixed in a testing rig (providing a reaction torque); while testing position control, each joint was free to rotate. The knee and ankle were tested separately, and series elasticity was not included in these initial tests. All data were recorded by the higher level control system, at ~750 Hz.

A. Step Response

Step response tests were conducted to quantify the OSL's ability to track a change in reference. Motor encoder step responses were recorded at 5º, 10º, and 15º, in joint coordinates. Step responses were commanded from the midpoint of each joint's range of motion. Similarly, motor current step responses were recorded at 2 A, 4 A, and 6 A phase-to-phase, corresponding to 1.2 A, 2.3 A, and 3.5 A using the common brushed DC electromechanical model, respectively. Current responses were commanded near the end of each joint's range of motion, while the joint was mechanically grounded. These current commands correspond to approximately 6 Nm, 12 Nm, and 18 Nm for the knee, and 9 Nm, 18 Nm, and 27 Nm for the ankle, based on the ankle's kinematic dependency of transmission ratio.

B. Frequency Response

Frequency response tests were conducted to quantify the range of frequencies in which the OSL can track a reference command. To estimate the frequency response, the reference command was a Gaussian white noise signal (3rd order, 40 Hz low-pass filtered for the position signal). This signal was scaled to test frequency response for a peak joint position at 5º, 10º, and 15º amplitudes, and a peak motor current at 1.2 A, 2.3 A, and 3.5 A, for the position and current controllers, respectively. Data were collected for 15 s and 60 s for the position and current tests, respectively. Bode plots were determined using Blackman-Tukey spectral analysis, where the auto-spectrum and cross-spectrum are divided in the frequency domain [34].

IV. Characterization Results

A. Step Response

Time-domain characterization of motor position and motor current shows consistent, repeatable step responses across a range of step sizes (Table I, Fig. 5). Furthermore,

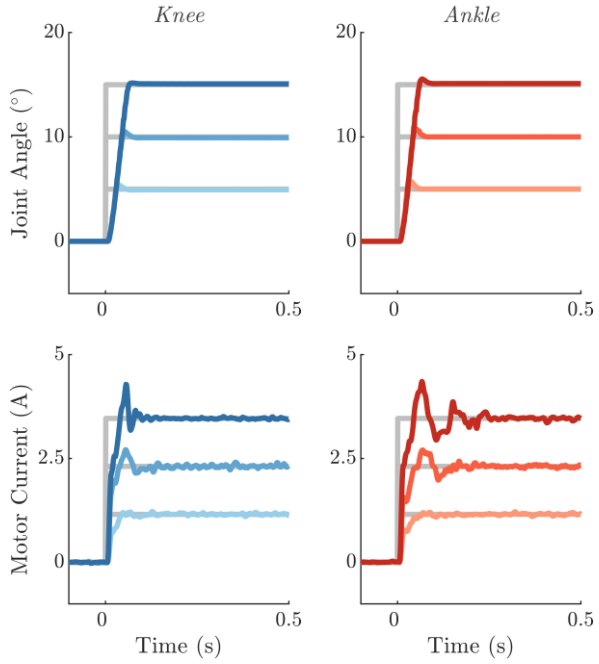

Fig. 5. Joint position (top) and motor current (bottom) step responses for the knee (left) and ankle (right) prostheses.

joint position step responses are consistent across the knee and ankle range of motion.

B. *Frequency Response*

The Bode plots of the frequency response demonstrate that controller performance varies with amplitude (Table I, Fig. 6). Overall, joint position and motor current bandwidths were 10-20 Hz and over 200 Hz, respectively (Table I); therefore, the OSL is capable of high-fidelity tracking commanded angles and currents below these frequencies. Able-bodied knee and ankle kinetic data during walking exhibit significant frequencies at or below 3.5 Hz—well below the bandwidth of the OSL [5].

V. Discussion

In this paper, we introduced the design of the Open-source Leg (OSL) prosthesis and characterized controller performance in the time and frequency domains. The OSL is a simple, portable, scalable, customizable, and economical testing platform. The intent of the OSL is to provide an accessible hardware platform for evaluation of prosthesis control strategies within the lab, community, and at home.

The OSL was designed to meet the kinematics and kinetics of able-bodied locomotion across a range of ambulation modes, including level ground walking and stair ascent/descent. These biomechanical demands were met using a high-torque electric motor coupled to a multi-stage timing belt drive transmission, as well as a linkage mechanism implemented in the ankle design. The knee can be configured as an SEA, with selectable series elasticity using custom torsional springs, or as a non-SEA. Finally, the clamshell-style housings provide structural support, safety, and belt tensioning capabilities.

A. *Comparison to Other Prostheses*

Technical specifications on some previously developed robotic prostheses can be limited. There are a number of previously developed robotic legs; however, depending on their application and preferences of their designers, some technical characteristics are not studied. This adds to the difficulty in cross-comparison across prosthesis hardware and limits the direct comparison of the prosthesis hardware itself.

Low transmission ratios are important in robotic prostheses because they govern size, electrical power demands, bandwidth, and audible noise, which ultimately impact mass, battery size, controllability, and other factors. The motor's high torque density enabled transmission ratios in the OSL to be 2-5 times lower than in other robotic prostheses [10], [11], [15], [17], [31]. Mass and size are also critical parameters for the success of prosthetic legs. Heavier prostheses require additional metabolic energy expenditure during movement, whereas longer prostheses can only be worn by tall amputees or those with a short residual limb length [35]. The overall mass of the OSL (~4000 g) is lower than most robotic knee/ankle prostheses, which typically have a mass of approximately 5000 g [15], [17], [31]. One notable exception is the knee/ankle prosthesis developed at the University of Utah, with a mass of 2845 g [10], [11].

The range of motion of the ankle joint within the OSL may be limited for some tasks. For most ambulation modes, the human ankle's range of motion is approximately 30º; however, during stair ascent/descent, some subjects require a range of motion up to 45º [28]. To accommodate this, the ankle prostheses developed at Vanderbilt and MIT have a range of motion of 70º and 45º, respectively [3], [15]. The range of motion for the ankle joint within the OSL is 30º,

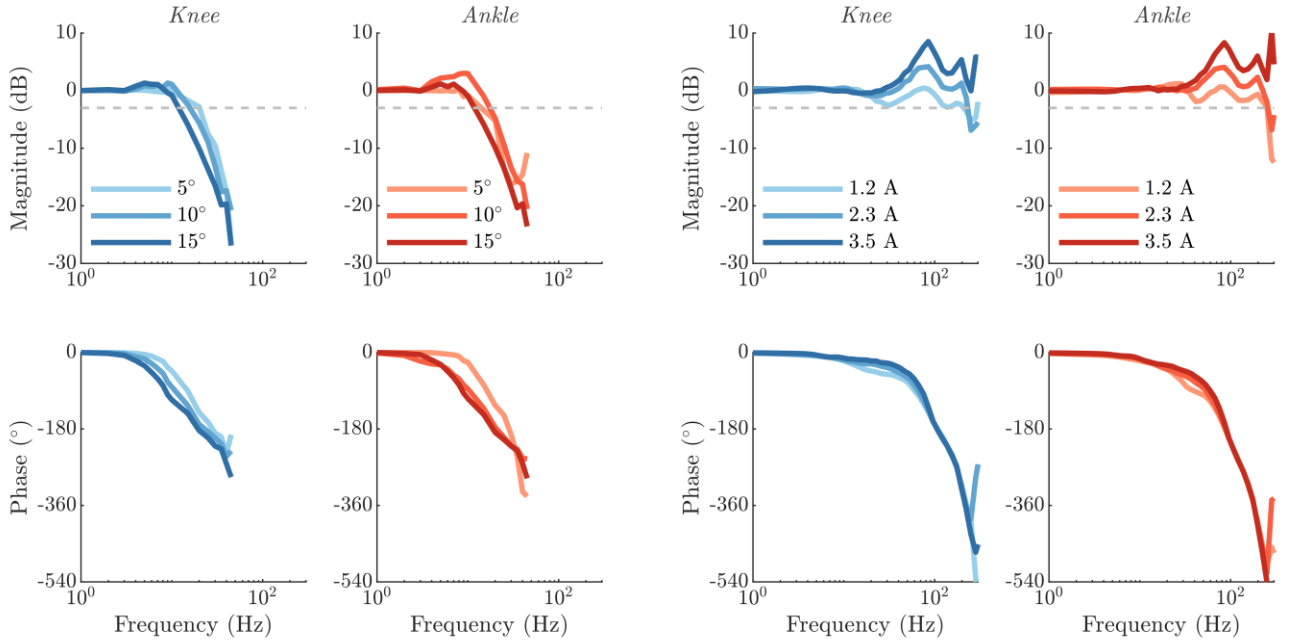

Fig. 6. Joint position (left) and motor current (right) Bode plots for the knee and ankle. Bandwidth is the frequency with a magnitude of -3 dB (dashed line).

and is limited by the kinematics of the four-bar linkage. This range of motion could be increased by decreasing the ankle's transmission ratio or by using a different transmission design. The knee joint within the OSL has a range of motion that is equal to that of other prosthetic knees and is far higher than the 70-90º needed for ambulation [15], [17], [36].

Recently developed prosthesis emulator systems offer an excellent alternative for quickly and systematically testing control systems in the laboratory [23]. Emulators couple lightweight prostheses with off-board motors via Bowden cables, leading to some of the best performance in terms of size, mass (45% lighter than the OSL ankle), torque, and bandwidth. Although emulator systems provide better performance, they must remain tethered to the off-board power source and are restricted to treadmill testing. The OSL was designed to be untethered from external hardware, enabling experiments outside of the lab and in more realistic environments, such as the community and home.

B. Future Work and Accessibility

Future work includes advancement of the embedded control systems, development of torque controllers that leverage series elasticity and the six-axis load cell, and testing with amputees utilizing the OSL. In addition, future work will include the development of dissemination materials and accessibility, including through the Neurobionics Lab website[1] at the University of Michigan. Available materials may include solid modeling files, bill of materials, links to suppliers, control system code, instructional guides, videos on assembly/disassembly, and any other relevant information to improve the usability of the OSL. Furthermore, an online forum can allow researchers to post questions, ideas, results, or independently-developed modifications.

ACKNOWLEDGMENT

The authors would like to thank J. F. Duval, T. Sharkey, and M. Mongeon for their assistance with FlexSEA, mechanical design, software.

REFERENCES

[1] K. Ziegler-Graham *et al.*, "Estimating the Prevalence of Limb Loss in the United States: 2005 to 2050," *Arch. Phys. Med. Rehabil.*, vol. 89, no. 3, pp. 422–429, 2008.

[2] R. L. Waters *et al.*, "Energy cost of walking of amputees: the influence of level of amputation.," *J. Bone Joint Surg. Am.*, vol. 58, no. 1, pp. 42–46, 1976.

[3] S. K. Au and H. M. Herr, "Powered ankle-foot prosthesis," *IEEE Robot. Autom. Mag.*, vol. 15, no. 3, pp. 52–59, 2008.

[4] W. C. Miller *et al.*, "The prevalence and risk factors of falling and fear of falling among lower extremity amputees," *Arch. Phys. Med. Rehabil.*, vol. 82, no. 8, pp. 1031–1037, 2001.

[5] D. A. Winter, *Biomechanics and Motor Control of Human Movement*, 4th ed. Hoboken, NJ: Wiley, 2009.

[6] R. Riener *et al.*, "Stair ascent and descent at different inclinations," *Gait Posture*, vol. 15, no. 1, pp. 32–44, 2002.

[7] L. Nolan *et al.*, "Adjustments in gait symmetry with walking speed in trans-femoral and trans-tibial amputees," *Gait Posture*, vol. 17, no. 2, pp. 142–151, 2003.

[8] D. A. Winter and S. E. Sienko, "Biomechanics of below-knee amputee gait," *J. Biomech.*, vol. 21, no. 5, pp. 361–367, 1988.

[9] R. Gailey *et al.*, "Review of secondary physical conditions associated with lower-limb amputation and long-term prosthesis use.," *J. Rehabil. Res. Dev.*, vol. 45, no. 1, pp. 15–29, 2008.

[10] T. Lenzi *et al.*, "Actively variable transmission for robotic knee prostheses," *Proc. - IEEE Int. Conf. Robot. Autom.*, pp. 6665–6671, 2017.

[11] T. Lenzi *et al.*, "A lightweight robotic ankle prosthesis with non-backdrivable cam-based transmission," *IEEE Int. Conf. Rehabil. Robot.*, pp. 1142–1147, 2017.

[12] P. Cherelle *et al.*, "Design and validation of the ankle mimicking prosthetic (AMP-) Foot 2.0," *IEEE Trans. Neural Syst. Rehabil. Eng.*, vol. 22, no. 1, pp. 138–148, 2014.

[13] Q. Wang *et al.*, "Walk the walk: A lightweight active transtibial prosthesis," *IEEE Robot. Autom. Mag.*, vol. 22, no. 4, pp. 80–89, 2015.

[14] F. Sup *et al.*, "Design and control of a powered knee and ankle prosthesis," *Proc. - IEEE Int. Conf. Robot. Autom.*, no. April, pp. 4134–4139, 2007.

[15] B. E. Lawson *et al.*, "A robotic leg prosthesis: Design, control, and implementation," *IEEE Robot. Autom. Mag.*, vol. 21, no. 4, pp. 70–81, 2014.

[16] S. K. Au *et al.*, "Powered ankle-foot prosthesis improves walking metabolic economy," *IEEE Trans. Robot.*, vol. 25, no. 1, pp. 51–66, 2009.

[17] E. J. Rouse *et al.*, "Clutchable series-elastic actuator: Implications for prosthetic knee design," *Int. J. Robot. Res.* , vol. 33, pp. 1611–1625, 2014.

[18] J. K. Hitt *et al.*, "An Active Foot-Ankle Prosthesis With Biomechanical Energy Regeneration," *J. Med. Device.*, vol. 4, no. 1, p. 011003, 2010.

[19] D. Quintero *et al.*, "Preliminary Experiments with a Unified Controller for a Powered Knee-Ankle Prosthetic Leg Across Walking Speeds," *IEEE Int. Conf. Intell. Robot. Syst.*, 2016.

[20] N. Thatte and H. Geyer, "Toward balance recovery with leg prostheses using neuromuscular model control," *IEEE Trans. Biomed. Eng.*, vol. 63, no. 5, pp. 904–913, 2016.

[21] M. Liu *et al.*, "Improving Finite State Impedance Control of Active-Transfemoral Prosthesis Using Dempster-Shafer Based State Transition Rules," *J. Intell. Robot. Syst. Theory Appl.*, vol. 76, no. 3–4, pp. 461–474, 2014.

[22] H. Zhao *et al.*, "Multicontact Locomotion on Transfemoral Prostheses via Hybrid System Models and Optimization-Based Control," *IEEE Trans. Autom. Sci. Eng.*, vol. 13, no. 2, pp. 502–513, 2016.

[23] J. M. Caputo and S. H. Collins, "A universal ankle-foot prosthesis emulator for human locomotion experiments," *J. Biomech. Eng.*, vol. 136, no. 3, p. 035002, 2014.

[24] M. R. Tucker *et al.*, "Control Strategies for Active Lower Extremity Prosthetics and Orthotics : A Review," *J. Neuroeng. Rehabil.*, no. January 2015, 2015.

[25] L. J. Hargrove *et al.*, "Robotic leg control with EMG decoding in an amputee with nerve transfers.," *N. Engl. J. Med.*, vol. 369, no. 13, pp. 1237–42, 2013.

[26] A. M. Simon *et al.*, "Configuring a powered knee and ankle prosthesis for transfemoral amputees within five specific ambulation modes," *PLoS One*, vol. 9, no. 6, 2014.

[27] E. J. Rouse *et al.*, "The design of a lightweight, low cost robotic knee prosthesis with selectable series elasticity," in *IEEE International Conference on Biomedical Robotics and Biomechatronics*, 2016.

[28] G. Bovi *et al.*, "A multiple-task gait analysis approach: kinematic, kinetic and EMG reference data for healthy young and adult subjects.," *Gait Posture*, vol. 33, no. 1, pp. 6–13, 2011.

[29] Stock Drive Products/Sterling Instrument (SDP/SI), "Handbook of Timing Belts, Pulleys, Chains and Sprockets."

[30] G. A. Pratt and M. M. Williamson, "Series Elastic Actuators," in *IEEE/RSJ International Conference on Intelligent Robots and Systems*, 1995, pp. 399–406.

[31] S. K. Au *et al.*, "Biomechanical Design of Powered Ankle-Foot Prosthesis," in *Proceedings of the IEEE 10th International Conference on Rehabilitation Robotics*, 2007, pp. 298–303.

[32] J. F. Duval and H. M. Herr, "FlexSEA: Flexible, Scalable Electronics Architecture for wearable robotic applications," *Proc. IEEE RAS*

[1] https://neurobionics.engin.umich.edu/

EMBS Int. Conf. Biomed. Robot. Biomechatronics, pp. 1236–1241, 2016.

[33] J. F. Duval and H. M. Herr, "FlexSEA-Execute: Advanced motion controller for wearable robotic applications," *Proc. IEEE RAS EMBS Int. Conf. Biomed. Robot. Biomechatronics*, pp. 1056–1061, 2016.

[34] L. Ljung, *System Identification: Theory for the User*, Second Ed. Upper Saddle River, NJ: Prentice Hall PTR, 1999.

[35] R. C. Browning *et al.*, "The effects of adding mass to the legs on the energetics and biomechanics of walking," *Med. Sci. Sports Exerc.*, vol. 39, no. 3, pp. 515–525, 2007.

[36] B. E. Lawson *et al.*, "Control of stair ascent and descent with a powered transfemoral prosthesis," *IEEE Trans. Neural Syst. Rehabil. Eng.*, vol. 21, no. 3, pp. 466–473, 2013.